PERGAMON

International Journal of Solids and Structures 40 (2003) 5799–5817

INTERNATIONAL JOURNAL OF SOLIDS and STRUCTURES

www.elsevier.com/locate/ijsolstr

Non-homogeneous displacement jumps in strong embedded discontinuities

J. Alfaiate [a,*], A. Simone [b], L.J. Sluys [b]

[a] *Dept. Eng. Civil, Instituto Superior Técnico and ICIST, Av. Rovisco Pais, 1049-001 Lisboa, Portugal*

[b] *Department of Civil Engineering and Geosciences, Delft University of Technology, P.O. Box 5048, 2600 GA Delft, The Netherlands*

Received 8 December 2002

Abstract

In this paper, strong discontinuities are embedded in finite elements to describe fracture in quasi-brittle materials. A new numerical formulation is introduced in which the displacement jumps do not need to be homogeneous within each finite element. Both the crack path and the displacement jumps are continuous across element boundaries. This formulation is compared with the discrete approach, in which interface elements are inserted to model the discontinuities, as well as with other embedded discontinuity approaches and with the partition of unity method. Numerical results have been obtained with relatively coarse meshes, which compare well with experimental results and with the results obtained from analyzes with interface elements.

Keywords: Strong embedded discontinuity; Discrete cracking

1. Introduction

In recent works, significant effort has been undertaken to model cracks as displacement discontinuities within a continuum. The embedded discontinuity formulations are examples of these contributions. Departing from the weak formulation, where discontinuities are modeled as finite width bands and the displacement field remains continuous, strong embedded discontinuities were introduced, in which the kinematics of a discontinuous displacement field is approximated. Many examples of the strong discontinuity approach can be found in literature, Dvorkin et al. (1990), Klisinski et al. (1991), Simo et al. (1993), Lotfi and Shing (1995), Armero and Garikipati (1996), Larsson and Runesson (1996), Oliver (1996a,b), Ohlsson and Olofsson (1997), Jirásek and Zimmermann (2001a,b), Wells and Sluys (2000), Borja (2000), Wells and Sluys (2001b), Alfaiate et al. (2001a), which are compared and discussed in Jirásek (2000). However, in these works, constant displacement jumps are adopted within each parent finite element. As a result, the jumps are not continuous across the element boundaries. In other approaches, like the extended

* Corresponding author. Tel.: +351-21-849-7650.

E-mail addresses: alfaiate@civil.ist.utl.pt (J. Alfaiate), a.simone@citg.tudelft.nl (A. Simone), l.j.sluys@citg.tudelft.nl (L.J. Sluys).

0020-7683/$ - see front matter © 2003 Elsevier Ltd. All rights reserved.
doi:10.1016/S0020-7683(03)00372-X

finite element method (XFEM) and the partition of unity method (Melenk and Babuška, 1996; Duarte and Oden, 1996; Babuška and Melenk, 1997; Möes et al., 1999; Wells and Sluys, 2001a) the possibility of interpolating a field over a body using partitions of unity is explored. In the works presented in Möes et al. (1999), Wells and Sluys (2001a) the jumps are modeled by additional global degrees of freedom located at the standard element nodes. As a consequence, continuous jumps across element boundaries can be obtained, but the concept of embedded discontinuities is no longer addressed.

In this paper, strong discontinuities are embedded in finite elements to describe fracture in quasi-brittle materials. First, a review of the variational formulation is presented as a common basis for both the current approach and the partition of unity method. Next, a new numerical formulation is introduced in which the displacement jumps at the discontinuities do not need to be constant functions within each element. The displacement jumps are approximated by additional degrees of freedom which are evaluated directly at the discontinuity surface. Continuity of the crack path is enforced and the displacement jumps are continuous across element boundaries. This formulation is compared with other approaches, namely the discrete one, in which interface elements are inserted to model the discontinuities (designated by discrete-interface approach in the remainder of the paper), other embedded discontinuity approaches and the partition of unity method. Numerical examples are presented, and the corresponding results are compared with experimental results and with the results obtained with other discontinuity models.

2. Kinematics of a discontinuity

In this section, the kinematics of the displacement and strain fields of a continuum crossed by a discontinuity are reviewed. The tensor notation is adopted. A strong discontinuity is characterized by a jump on the displacement field, localized at a surface. Consider a domain Ω, with boundary $\partial\Omega$ where a discontinuity surface Γ_{d} is supposed to exist (Fig. 1). External tractions are applied at part Γ_{t} of the boundary whereas displacements are imposed on part Γ_u of $\partial\Omega$, such that $\Gamma_{\mathrm{t}} \cup \Gamma_u = \partial\Omega$ and $\Gamma_{\mathrm{t}} \cap \Gamma_u = \emptyset$. The total displacement field is the sum of a continuous part on Ω, $\hat{\mathbf{u}}$, with a discontinuous part corresponding to the displacement jump $[\![\mathbf{u}]\!]$, localized at the discontinuity surface Γ_{d}:

$$\mathbf{u}(\mathbf{x}) = \hat{\mathbf{u}}(\mathbf{x}) + \mathscr{H}_{\Gamma_{\mathrm{d}}}[\![\mathbf{u}(\mathbf{x})]\!], \tag{1}$$

where $\mathscr{H}_{\Gamma_{\mathrm{d}}}$ is defined as

$$\mathscr{H}_{\Gamma_{\mathrm{d}}} = H_{\Gamma_{\mathrm{d}}} - (1 - r), \quad 0 \leqslant r \leqslant 1, \tag{2}$$

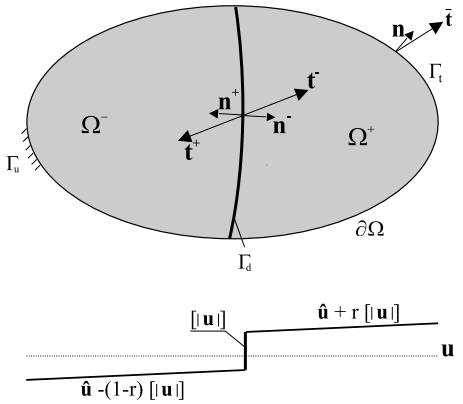

Fig. 1. Domain Ω crossed by a discontinuity surface Γ_{d}.

and H_{Γ_d} is the Heaviside function at the discontinuity Γ_d,

$$H_{\Gamma_d} = \begin{cases} 1 & \text{if } \mathbf{x} \in \Omega^+, \\ 0 & \text{otherwise.} \end{cases} \tag{3}$$

Similar to the works presented in Klisinski et al. (1991), Ohlsson and Olofsson (1997), Lotfi and Shing (1995), the scalar parameter r defines how the jump is transmitted to the the domain Ω: if $r = 1$ the jump is fully transmitted from Ω^- to Ω^+.

The strain field obtained from the continuous part of the displacement field is:

$$\hat{\boldsymbol{\varepsilon}} = \nabla^s \hat{\mathbf{u}} \quad \text{in } \Omega \setminus \Gamma_d, \tag{4}$$

where $(\cdot)^s$ refers to the symmetric part of $(\cdot)$. The total strain in the body is given by:

$$\boldsymbol{\varepsilon} = \nabla^s \mathbf{u} = \nabla^s \hat{\mathbf{u}} + \mathscr{H}_{\Gamma_d}(\nabla^s [\![\mathbf{u}]\!]) \quad \text{in } \Omega \setminus \Gamma_d, \tag{5}$$

$$\boldsymbol{\varepsilon} = \nabla^s \mathbf{u} = \underbrace{\nabla^s \hat{\mathbf{u}} + \mathscr{H}_{\Gamma_d}(\nabla^s [\![\mathbf{u}]\!])}_{\text{bounded}} + \underbrace{\delta_{\Gamma_d}([\![\mathbf{u}]\!] \otimes \mathbf{n})^s}_{\text{unbounded}} \quad \text{in } \Omega, \tag{6}$$

where $\otimes$ denotes a dyadic product and δ_{Γ_d} is the Dirac delta-function along surface Γ_d. Both the displacement field and the strain field are continuous in Ω^- and Ω^+, since the unbounded term in Eq. (6) vanishes in $\Omega \setminus \Gamma_d = \Omega^- \cup \Omega^+$.

3. Variational formulation

In this section, the variational formulation is reviewed as a common basis for various discrete approaches, namely strong embedded discontinuities (Dvorkin et al., 1990; Klisinski et al., 1991; Simo et al., 1993; Lotfi and Shing, 1995; Armero and Garikipati, 1996; Larsson and Runesson, 1996; Oliver, 1996a,b; Ohlsson and Olofsson, 1997; Jirásek and Zimmermann, 2001a,b; Wells and Sluys, 2000; Borja, 2000; Wells and Sluys, 2001b; Alfaiate et al., 2001a) and the partition of unity method (Melenk and Babuška, 1996; Duarte and Oden, 1996; Babuška and Melenk, 1997; Möes et al., 1999; Wells and Sluys, 2001a). Consider Ω the domain occupied by the body represented in Fig. 1, as described in Section 2. In the following, similar to the works presented in Simo et al. (1993), Lotfi and Shing (1995) and Wells (2001), the extension of the three-field Hu-Washizu variational statements (Washizu, 1982) to a body containing an internal discontinuity surface is first considered. Next, the principle of virtual work extended for a cracked body will be obtained as a particular case. In the following, $(\cdot)$ and $(:)$ refer to single and double contractions, respectively.

The governing field equations are imposed separately in $\Omega \setminus \Gamma_d$ and on Γ_d. Together with the boundary conditions, they can be expressed as (see Fig. 1):

$$\nabla \cdot \boldsymbol{\sigma} + \mathbf{b} = \mathbf{0} \quad \text{in } \Omega \setminus \Gamma_d, \tag{7}$$

$$\boldsymbol{\varepsilon} = \nabla^s \mathbf{u} \quad \text{in } \Omega \setminus \Gamma_d, \tag{8}$$

$$\boldsymbol{\sigma} = \boldsymbol{\sigma}(\boldsymbol{\varepsilon}) \quad \text{in } \Omega \setminus \Gamma_d, \tag{9}$$

$$\mathbf{u} = \bar{\mathbf{u}} \quad \text{at } \Gamma_u, \tag{10}$$

$$\boldsymbol{\sigma} \cdot \mathbf{n} = \bar{\mathbf{t}} \quad \text{at } \Gamma_t, \tag{11}$$

$$\boldsymbol{\sigma}^+ \cdot \mathbf{n}^+ = \mathbf{t}^+ \quad \text{at } \Gamma_d, \tag{12}$$

$$\boldsymbol{\sigma}^- \cdot \mathbf{n}^- = \mathbf{t}^- \quad \text{at } \Gamma_d, \tag{13}$$

$$\mathbf{t}^+ = -\mathbf{t}^- = \mathbf{t} \quad \text{at } \Gamma_d, \tag{14}$$

where $\mathbf{b}$ are the body forces and $\bar{\mathbf{u}}$ and $\bar{\mathbf{t}}$ are the prescribed displacements and tractions at the boundary, respectively. Eq. (8) is the strain displacement relation and Eq. (9) is the constitutive law. Eqs. (12) and (13) enforce traction continuity across the discontinuity surface Γ_d, where the tractions are denoted by $\mathbf{t}$. As depicted in Fig. 1, $\mathbf{n}^+ = -\mathbf{n}^-$, is the outward normal of Ω^+ and $\mathbf{t}^+ = -\mathbf{t}^-$ denotes the traction vector acting on Ω^+.

Eqs. (7)–(13) can be defined separately in sub-domains Ω^+ and Ω^-. Assuming that the essential boundary conditions are satisfied ($\mathbf{u} = \bar{\mathbf{u}}$ at Γ_u), the following weak form is obtained:

$$\begin{aligned}
&\int_{\Omega^-} \delta\mathbf{u} \cdot (\nabla \cdot \boldsymbol{\sigma} + \mathbf{b})\, d\Omega + \int_{\Omega^+} \delta\mathbf{u} \cdot (\nabla \cdot \boldsymbol{\sigma} + \mathbf{b})\, d\Omega + \int_{\Omega^-} \delta\boldsymbol{\sigma} : (\boldsymbol{\varepsilon} - \nabla^s \mathbf{u})\, d\Omega + \int_{\Omega^+} \delta\boldsymbol{\sigma} : (\boldsymbol{\varepsilon} - \nabla^s \mathbf{u})\, d\Omega \\
&\quad + \int_{\Gamma_t^-} \delta\mathbf{u} \cdot (\bar{\mathbf{t}} - \boldsymbol{\sigma} \cdot \mathbf{n})\, d\Gamma + \int_{\Gamma_t^+} \delta\mathbf{u} \cdot (\bar{\mathbf{t}} - \boldsymbol{\sigma} \cdot \mathbf{n})\, d\Gamma + \int_{\Omega^-} \delta\boldsymbol{\varepsilon} : (\boldsymbol{\sigma} - \boldsymbol{\sigma}(\boldsymbol{\varepsilon}))\, d\Omega + \int_{\Omega^+} \delta\boldsymbol{\varepsilon} : (\boldsymbol{\sigma} - \boldsymbol{\sigma}(\boldsymbol{\varepsilon}))\, d\Omega \\
&\quad + \int_{\Gamma_d} \delta\mathbf{u}^+ \cdot (\mathbf{t}^+ - \boldsymbol{\sigma}^+ \cdot \mathbf{n}^+)\, d\Gamma + \int_{\Gamma_d} \delta\mathbf{u}^- \cdot (\mathbf{t}^- - \boldsymbol{\sigma}^- \cdot \mathbf{n}^-)\, d\Gamma = 0,
\end{aligned} \tag{15}$$

where $\delta\mathbf{u}$, $\delta\boldsymbol{\varepsilon}$ and $\delta\boldsymbol{\sigma}$ denote compatible variations of the total displacements, strains and stresses, respectively.

At this stage, it is possible to consider $\mathbf{u}$, $\boldsymbol{\varepsilon}$, $\boldsymbol{\sigma}$, $[\![\mathbf{u}]\!]$ as independent unknown fields. This possibility was explored in Lotfi and Shing (1995), where mixed finite elements were proposed to approximate the independent unknown fields. In the adopted approach, Eq. (8) is automatically satisfied due to (5). Using the divergence theorem in sub-domains Ω^- and Ω^+, one obtains:

$$\int_{\Omega^-} \delta\mathbf{u} \cdot (\nabla \cdot \boldsymbol{\sigma})\, d\Omega = -\int_{\Omega^-} (\nabla^s \delta\mathbf{u}) : \boldsymbol{\sigma}\, d\Omega + \int_{\Gamma_t^-} \delta\mathbf{u} \cdot (\boldsymbol{\sigma} \cdot \mathbf{n})\, d\Gamma + \int_{\Gamma_d} \delta\mathbf{u}^- \cdot (\boldsymbol{\sigma}^- \cdot \mathbf{n}^-)\, d\Gamma, \tag{16}$$

$$\int_{\Omega^+} \delta\mathbf{u} \cdot (\nabla \cdot \boldsymbol{\sigma})\, d\Omega = -\int_{\Omega^+} (\nabla^s \delta\mathbf{u}) : \boldsymbol{\sigma}\, d\Omega + \int_{\Gamma_t^+} \delta\mathbf{u} \cdot (\boldsymbol{\sigma} \cdot \mathbf{n})\, d\Gamma + \int_{\Gamma_d} \delta\mathbf{u}^+ \cdot (\boldsymbol{\sigma}^+ \cdot \mathbf{n}^+)\, d\Gamma, \tag{17}$$

where $\Gamma_t^+ = \Gamma_t \cap \partial\Omega^+$ and $\Gamma_t^- = \Gamma_t \cap \partial\Omega^-$. The weak form (15) can now be written as

$$\begin{aligned}
&-\int_{\Omega \setminus \Gamma_d} (\nabla^s \delta\mathbf{u}) : \boldsymbol{\sigma}\, d\Omega + \int_{\Omega \setminus \Gamma_d} \delta\mathbf{u} \cdot \mathbf{b}\, d\Omega + \int_{\Gamma_t} \delta\mathbf{u} \cdot \bar{\mathbf{t}}\, d\Gamma \\
&\quad + \int_{\Omega \setminus \Gamma_d} \delta\boldsymbol{\varepsilon} : (\boldsymbol{\sigma} - \boldsymbol{\sigma}(\boldsymbol{\varepsilon}))\, d\Omega + \int_{\Gamma_d} (\delta\mathbf{u}^+ - \delta\mathbf{u}^-) \cdot \mathbf{t}^+\, d\Gamma = 0.
\end{aligned} \tag{18}$$

Recalling Eqs. (1) and (6) and taking the variations of the total displacements equal to

$$\delta\mathbf{u} = \delta\hat{\mathbf{u}} + \mathscr{H}_{\Gamma_d}\, \delta[\![\mathbf{u}]\!], \tag{19}$$

the variations of the strain equal to

$$\delta\boldsymbol{\varepsilon} = \nabla^s \delta\hat{\mathbf{u}} + \mathscr{H}_{\Gamma_d} \nabla^s \delta[\![\mathbf{u}]\!] \quad \text{in } \Omega \setminus \Gamma_d, \tag{20}$$

and the variations of the jumps given by

$$\delta[\![\mathbf{u}]\!] = \delta\mathbf{u}^+ - \delta\mathbf{u}^- \quad \text{at } \Gamma_d, \tag{21}$$

one obtains:

$$
\begin{aligned}
&-\int_{\Omega\setminus\Gamma_d}(\nabla^s\delta\hat{\mathbf{u}}):\boldsymbol{\sigma}\,d\Omega-\int_{\Omega\setminus\Gamma_d}\mathscr{H}_{\Gamma_d}(\nabla^s\delta[\![\mathbf{u}]\!]):\boldsymbol{\sigma}\,d\Omega\\
&+\int_{\Omega\setminus\Gamma_d}\delta\hat{\mathbf{u}}\cdot\mathbf{b}\,d\Omega+\int_{\Omega\setminus\Gamma_d}\mathscr{H}_{\Gamma_d}\delta[\![\mathbf{u}]\!]\cdot\mathbf{b}\,d\Omega\\
&+\int_{\Gamma_t}\delta\hat{\mathbf{u}}\cdot\bar{\mathbf{t}}\,d\Gamma+\int_{\Gamma_t}\mathscr{H}_{\Gamma_d}\delta[\![\mathbf{u}]\!]\cdot\bar{\mathbf{t}}\,d\Gamma\\
&+\int_{\Omega\setminus\Gamma_d}(\nabla^s\delta\hat{\mathbf{u}}):(\boldsymbol{\sigma}-\boldsymbol{\sigma}(\boldsymbol{\varepsilon}))\,d\Omega+\int_{\Omega\setminus\Gamma_d}\mathscr{H}_{\Gamma_d}(\nabla^s\delta[\![\mathbf{u}]\!]):(\boldsymbol{\sigma}-\boldsymbol{\sigma}(\boldsymbol{\varepsilon}))\,d\Omega\\
&+\int_{\Gamma_d}\delta[\![\mathbf{u}]\!]\cdot\mathbf{t}^+\,d\Gamma=0,
\end{aligned}
\tag{22}
$$

which reduces to

$$
\begin{aligned}
&-\int_{\Omega\setminus\Gamma_d}(\nabla^s\delta\hat{\mathbf{u}}):\boldsymbol{\sigma}(\boldsymbol{\varepsilon})\,d\Omega-\int_{\Omega\setminus\Gamma_d}\mathscr{H}_{\Gamma_d}(\nabla^s\delta[\![\mathbf{u}]\!]):\boldsymbol{\sigma}(\boldsymbol{\varepsilon})\,d\Omega\\
&+\int_{\Omega\setminus\Gamma_d}\delta\hat{\mathbf{u}}\cdot\mathbf{b}\,d\Omega+\int_{\Omega\setminus\Gamma_d}\mathscr{H}_{\Gamma_d}\delta[\![\mathbf{u}]\!]\cdot\mathbf{b}\,d\Omega\\
&+\int_{\Gamma_t}\delta\hat{\mathbf{u}}\cdot\bar{\mathbf{t}}\,d\Gamma+\int_{\Gamma_t}\mathscr{H}_{\Gamma_d}\delta[\![\mathbf{u}]\!]\cdot\bar{\mathbf{t}}\,d\Gamma\\
&+\int_{\Gamma_d}\delta[\![\mathbf{u}]\!]\cdot\mathbf{t}^+\,d\Gamma=0.
\end{aligned}
\tag{23}
$$

Taking first $\delta[\![\mathbf{u}]\!]=\mathbf{0}$ and then $\delta\hat{\mathbf{u}}=\mathbf{0}$, and since the stress field in the continuum depends upon the regular strain $\hat{\boldsymbol{\varepsilon}}$,

$$
\boldsymbol{\sigma}=\boldsymbol{\sigma}(\hat{\boldsymbol{\varepsilon}}),
\tag{24}
$$

the following two variational statements can be obtained:

$$
-\int_{\Omega\setminus\Gamma_d}(\nabla^s\delta\hat{\mathbf{u}}):\boldsymbol{\sigma}(\hat{\boldsymbol{\varepsilon}})\,d\Omega+\int_{\Omega\setminus\Gamma_d}\delta\hat{\mathbf{u}}\cdot\mathbf{b}\,d\Omega+\int_{\Gamma_t}\delta\hat{\mathbf{u}}\cdot\bar{\mathbf{t}}\,d\Gamma=0,
\tag{25}
$$

$$
-\int_{\Omega}\mathscr{H}_{\Gamma_d}(\nabla^s\delta[\![\mathbf{u}]\!]):\boldsymbol{\sigma}(\hat{\boldsymbol{\varepsilon}})\,d\Omega+\int_{\Omega}\mathscr{H}_{\Gamma_d}\delta[\![\mathbf{u}]\!]\cdot\mathbf{b}\,d\Omega+\int_{\Gamma_t}\mathscr{H}_{\Gamma_d}\delta[\![\mathbf{u}]\!]\cdot\bar{\mathbf{t}}\,d\Gamma+\int_{\Gamma_d}\delta[\![\mathbf{u}]\!]\cdot\mathbf{t}^+\,d\Gamma=0.
\tag{26}
$$

In (26), the tractions are obtained from a separate traction-jump law at the discontinuity, such that $\mathbf{t}=\mathbf{t}([\![\mathbf{u}]\!])$.

Eq. (25) is the usual principle of virtual work obtained for a continuum. It is interesting to note that, taking $r=1$ in (2), this formulation is the same as the one adopted in the partition of unity method (Wells and Sluys, 2001a; Wells, 2001; Simone et al., 2000), in which case the second variational statement (26) can be interpreted as the principle of virtual work applied to subdomain Ω^+. More generally, if r is taken between 0 and 1, separate contributions in Ω^+ and Ω^- are taken into account, similar to the work presented in Lotfi and Shing (1995), Ohlsson and Olofsson (1997). Furthermore, summing Eqs. (25) and (26), the principle of virtual work applied to a body crossed by a discontinuity is recovered as presented in Malvern (1969), i.e.,

$$
-\int_{\Omega\setminus\Gamma_d}(\nabla^s\delta\mathbf{u}):\boldsymbol{\sigma}(\hat{\boldsymbol{\varepsilon}})\,d\Omega+\int_{\Gamma_d}\delta[\![\mathbf{u}]\!]\cdot\mathbf{t}^+\,d\Gamma+\int_{\Omega\setminus\Gamma_d}\delta\mathbf{u}\cdot\mathbf{b}\,d\Omega+\int_{\Gamma_t}\delta\mathbf{u}\cdot\bar{\mathbf{t}}\,d\Gamma=0,
\tag{27}
$$

which is the weak form usually adopted in the discrete-interface approach.

It is also interesting to compare the adopted variational formulation with the one introduced in Simo et al. (1993) and used in many other works, namely in Armero and Garikipati (1996), Oliver (1996b), Wells and Sluys (2001b), Jirásek and Zimmermann (2001a), Alfaiate et al. (2001a). In the latter case, two variational statements are also introduced: the first is the principle of virtual work (25) and the second, which is introduced at element level, is:

$$\frac{1}{l_{\mathrm{d}}}\int_{\Gamma_{\mathrm{d}}^{e}}\mathbf{t}\,\mathrm{d}\Gamma-\frac{1}{\Omega^{e}}\int_{\Omega^{e}}\sigma\cdot\mathbf{n}\,\mathrm{d}\Omega=\mathbf{0}, \tag{28}$$

where l_{d} is the length of the discontinuity Γ_{d}^{e} embedded in the parent element Ω^{e}. In Eq. (28), the traction continuity condition is imposed in average. It can be shown that, in the present formulation, the traction continuity condition is also enforced in a weak form through Eq. (26), although in a different way. Departing from the corresponding strong form:

$$\mathbf{t}-\sigma\cdot\mathbf{n}=\mathbf{0}, \tag{29}$$

pre-multiplying both sides of (29) by the variations of the jumps and integrating along Γ_{d} one obtains

$$\int_{\Gamma_{\mathrm{d}}}\delta[\![\mathbf{u}]\!]\cdot\mathbf{t}\,\mathrm{d}\Gamma-\int_{\Gamma_{\mathrm{d}}}\delta[\![\mathbf{u}]\!]\cdot(\sigma\cdot\mathbf{n})\,\mathrm{d}\Gamma=0. \tag{30}$$

Take, for example, $r=1$, such that $\delta\mathbf{u}^{+}=\delta[\![\mathbf{u}]\!]$, and $\delta\hat{\mathbf{u}}=\mathbf{0}$. Applying the divergence theorem to subdomain Ω^{+} as done in Eq. (17), one obtains

$$\int_{\Omega^{+}}(\nabla^{\mathrm{s}}\delta[\![\mathbf{u}]\!]):\boldsymbol{\sigma}\,\mathrm{d}\Omega=\int_{\Gamma_{\mathrm{t}}^{+}}(\delta[\![\mathbf{u}]\!])\cdot\bar{\mathbf{t}}\,\mathrm{d}\Gamma+\int_{\Gamma_{\mathrm{d}}}(\delta[\![\mathbf{u}]\!])\cdot(\boldsymbol{\sigma}^{+}\cdot\mathbf{n}^{+})\,\mathrm{d}\Gamma-\int_{\Omega^{+}}(\delta[\![\mathbf{u}]\!])\cdot(\nabla\cdot\boldsymbol{\sigma})\,\mathrm{d}\Omega, \tag{31}$$

or, equivalently

$$-\int_{\Gamma_{\mathrm{d}}}(\delta[\![\mathbf{u}]\!])\cdot(\boldsymbol{\sigma}^{+}\cdot\mathbf{n}^{+})\,\mathrm{d}\Gamma=-\int_{\Omega^{+}}(\nabla^{\mathrm{s}}\delta[\![\mathbf{u}]\!]):\boldsymbol{\sigma}\,\mathrm{d}\Omega+\int_{\Gamma_{\mathrm{t}}^{+}}(\delta[\![\mathbf{u}]\!])\cdot\bar{\mathbf{t}}\,\mathrm{d}\Gamma+\int_{\Omega^{+}}(\delta[\![\mathbf{u}]\!])\cdot\mathbf{b}\,\mathrm{d}\Omega. \tag{32}$$

From Eqs. (30), (32) and (14) we get Eq. (26). In Section 4, we shall see that a symmetric formulation can be obtained from (25) and (26) (as in the partition of unity method), instead of the non-symmetric formulation introduced by Simo et al. (1993).

4. Finite element approximation

Consider a finite element discretisation of the 2D domain Ω. Assume that one element is crossed by a straight discontinuity which divides Ω in two sub-domains Ω^{+} and Ω^{-} (Fig. 2).

Recall Eq. (1). The jump $[\![\mathbf{u}]\!]$ occurs along surface Γ_{d} within the element,

$$[\![\mathbf{u}]\!]=[\![\mathbf{u}(s(\mathbf{x}))]\!], \tag{33}$$

where $s(\mathbf{x})$ is the coordinate along Γ_{d} as depicted in Fig. 2(left). In this figure, a local frame s, n related to the discontinuity is defined, where n is the normal to the discontinuity. Assume the jump is a linear function of s given by:

$$[\![\mathbf{u}(s)]\!]=(D+qs)\mathbf{e}_{s}+(C+ks)\mathbf{e}_{n}, \tag{34}$$

where D, q, C and k are constants and $\mathbf{e}_{s}$ and $\mathbf{e}_{n}$ are unit vectors along directions s and n, respectively. For all $\mathbf{x}\in\Omega^{+}$, $r[\![\mathbf{u}(s)]\!]$ will be added to the displacement field $\hat{\mathbf{u}}$, whereas for all $\mathbf{x}\in\Omega^{-}$, $(1-r)[\![\mathbf{u}(s)]\!]$ will be subtracted from the displacement field $\hat{\mathbf{u}}$. In Fig. 2(right) the total displacement field is depicted (where $\hat{\mathbf{u}}$ and the tangential jump component are neglected for clarity). If the jump is assumed to be constant across

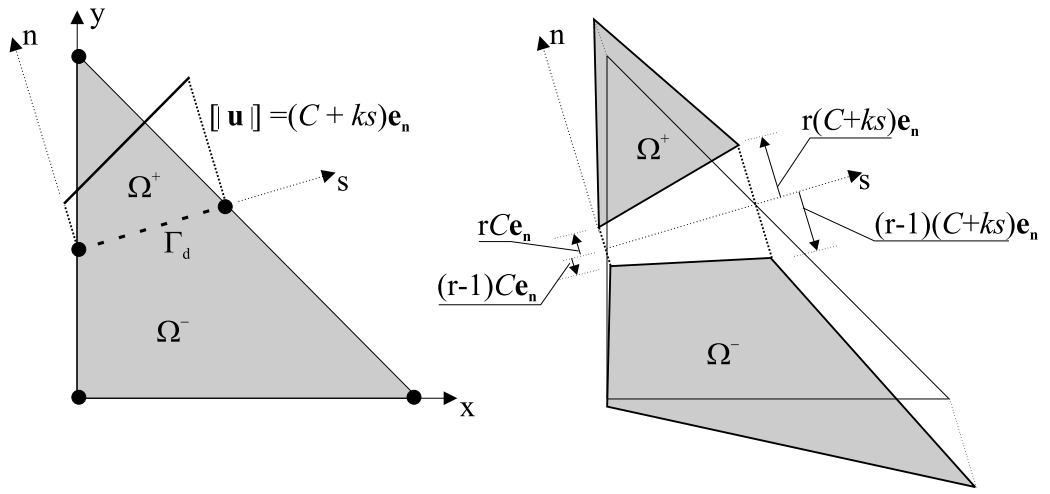

Fig. 2. Displacement jump in a triangle crossed by a discontinuity.

Γ_d, it is sufficient to adopt one internal node to represent the displacement jump; in the work presented in Alfaiate et al. (2001a), where crack path continuity was enforced, this node was introduced at the midpoint of Γ_d. However, if higher order functions are considered for $[\![\mathbf{u}]\!]$, more nodes are required: two nodes for a linear function, three nodes for a quadratic function and so forth. In the example above, the additional two nodes are located at the intersection of Γ_d with the edges of the element (if a quadratic function were adopted, a third node would be located at the midpoint of Γ_d).

In matrix form, for each finite element e with n nodes, the following approximation of the displacement field (1) is adopted:

$$\begin{aligned} &\hat{\mathbf{u}}^e = \mathbf{N}^e(\mathbf{x})\hat{\mathbf{a}}^e \quad \text{in } \Omega^e \setminus \Gamma_d^e, \\ &[\![\mathbf{u}]\!]^e = \mathbf{N}_w^e[s(\mathbf{x})]\mathbf{w}^e \quad \text{at } \Gamma_d^e, \end{aligned} \tag{35}$$

where $\mathbf{N}^e$ contains the usual element shape functions ψ_i^e, $1 \leqslant i \leqslant n$, $\hat{\mathbf{a}}^e$ are the nodal degrees of freedom associated with $\hat{\mathbf{u}}$, $\mathbf{N}_w^e$ are the shape functions used to approximate the jumps $[\![\mathbf{u}]\!]$ and $\mathbf{w}^e$ are the degrees of freedom associated with $[\![\mathbf{u}]\!]$. In (35), if the number of nodes used to approximate the jumps is n_w, $\mathbf{N}_w$ is a $(2 \times 2n_w)$ matrix: if $n_w = 1$, $\mathbf{N}_w$ is the identity matrix; if $n_w = 2$, $\mathbf{N}_w$ contains linear shape functions and so forth.

Assume that the total displacement field, $\mathbf{u} = \hat{\mathbf{u}} + \mathscr{H}_{\Gamma_d}[\![\mathbf{u}]\!]$, is approximated by the usual shape functions:

$$\mathbf{u}^e = \mathbf{N}^e(\mathbf{x})\mathbf{a}^e \quad \text{in } \Omega^e \setminus \Gamma_d^e, \tag{36}$$

where $\mathbf{a}^e$ are the nodal degrees of freedom associated with total displacements $\mathbf{u}$. Since the approximated displacement field is continuous, the contribution of the jump across discontinuity Γ_d into $\mathbf{u}^e$ must also be continuous. This can be achieved by projecting the jump to the n element nodes such that:

$$\mathscr{H}_{\Gamma_d}[\![\mathbf{u}]\!]^e \approx \mathbf{N}^e\mathbf{H}\tilde{\mathbf{a}}^e, \tag{37}$$

where $\mathbf{H}$ is a $(2n \times 2n)$ matrix, $\mathbf{H} = \mathscr{H}_{\Gamma_d}\mathbf{I}$, and $\mathbf{I}$ is the $(2n \times 2n)$ unit matrix. Thus, in $\mathbf{H}$ elements related to Ω^{e+} are equal to $(0 \leqslant r \leqslant 1)$ and elements related to Ω^{e-} are equal to $(r-1)$, i.e.,

$$H_{kl} = \begin{cases} 0 & \text{if } k \neq l, \\ 0 \leqslant r \leqslant 1 & \text{if } [(k = l = 2i-1) \vee (k = l = 2i)] \wedge \text{node } i \in \Omega^{e+}, \\ (r-1) & \text{if } [(k = l = 2j-1) \vee (k = l = 2j)] \wedge \text{node } j \in \Omega^{e-}. \end{cases} \tag{38}$$

The enhanced degrees of freedom $\tilde{\mathbf{a}}^e$ are given by

$$\tilde{\mathbf{a}}^e = \mathbf{M}_w^e \mathbf{w}^e. \tag{39}$$

In (39), $\mathbf{M}_w^e$ is a $(2n \times 2n_w)$ matrix:

$$\mathbf{M}_w^e = \begin{bmatrix} \mathbf{N}_{w1}^e \\ \mathbf{N}_{w2}^e \\ \cdots \\ \mathbf{N}_{wn}^e \end{bmatrix}, \tag{40}$$

where $\mathbf{N}_{wi}^e$ are the shape functions obtained at Γ_d for $s = s(\mathbf{x}_i)$, $\mathbf{x}_i$ being the coordinates of node i. As a result, the displacement field in each element is given by:

$$\begin{aligned} &\mathbf{u}^e = \mathbf{N}^e(\hat{\mathbf{a}}^e + \mathbf{H}\tilde{\mathbf{a}}^e) = \mathbf{N}^e(\hat{\mathbf{a}}^e + \mathbf{H}\mathbf{M}_w^e \mathbf{w}^e) \quad \text{in } \Omega^e, \\ &[\![\mathbf{u}]\!]^e = \mathbf{N}_w^e[s(\mathbf{x})]\mathbf{w}^e \quad \text{at } \Gamma_\mathrm{d}^e. \end{aligned} \tag{41}$$

The strain field $\hat{\boldsymbol{\varepsilon}}^e$ is approximated by:

$$\hat{\boldsymbol{\varepsilon}}^e = \mathbf{L}\mathbf{N}^e\hat{\mathbf{a}}^e = \mathbf{B}^e(\mathbf{a}^e - \mathbf{H}\mathbf{M}_w^e\mathbf{w}^e), \tag{42}$$

where $\mathbf{L}$ is the usual differential operator. The incremental stress field is

$$\mathrm{d}\boldsymbol{\sigma}^e = \mathbf{D}^e\,\mathrm{d}\hat{\boldsymbol{\varepsilon}}^e = \mathbf{D}^e\mathbf{B}^e(\mathrm{d}\mathbf{a}^e - \mathbf{H}\mathbf{M}_w^e\,\mathrm{d}\mathbf{w}^e). \tag{43}$$

The tractions are obtained from the traction-jump law at the discontinuity. In incremental format this reads:

$$\mathrm{d}\mathbf{t}^e = \mathbf{T}^e\,\mathrm{d}[\![\mathbf{u}]\!]^e = \mathbf{T}^e\mathbf{N}_w^e\,\mathrm{d}\mathbf{w}^e \quad \text{at } \Gamma_\mathrm{d}^e. \tag{44}$$

Discretising (25) and (26) by means of the field approximations given in (35)–(44), we obtain:

$$\begin{bmatrix} \mathbf{K}_{aa}^e & -\mathbf{K}_{aw}^e \\ -\mathbf{K}_{wa}^e & \mathbf{K}_{ww}^e + \mathbf{K}_\mathrm{d}^e \end{bmatrix} \begin{Bmatrix} \mathrm{d}\mathbf{a}^e \\ \mathrm{d}\mathbf{w}^e \end{Bmatrix} = \begin{Bmatrix} \mathrm{d}\mathbf{f}_\mathrm{ext}^e \\ \mathrm{d}\mathbf{f}_{w,\mathrm{ext}}^e \end{Bmatrix}, \tag{45}$$

where

$$\mathbf{K}_{aa}^e = \int_{\Omega^e} \mathbf{B}^{eT}\mathbf{D}^e\mathbf{B}^e\,\mathrm{d}\Omega, \tag{46}$$

$$\mathbf{K}_{aw}^e = \int_{\Omega^e} \mathbf{B}^{eT}\mathbf{D}^e\mathbf{B}_w^e\,\mathrm{d}\Omega, \tag{47}$$

$$\mathbf{K}_{wa}^e = \mathbf{K}_{aw}^{eT}, \tag{48}$$

$$\mathbf{K}_{ww}^e = \int_{\Omega^e} \mathbf{B}_w^{eT}\mathbf{D}^e\mathbf{B}_w^e\,\mathrm{d}\Omega, \tag{49}$$

$$\mathbf{K}_\mathrm{d}^e = \int_{\Gamma_\mathrm{d}} \mathbf{N}_w^{eT}\mathbf{T}^e\mathbf{N}_w^e\,\mathrm{d}\Gamma, \tag{50}$$

$$\mathbf{B}_w^e = \mathbf{B}^e\mathbf{H}\mathbf{M}_w^e, \tag{51}$$

and

$$\mathrm{d}\mathbf{f}_\mathrm{ext}^e = \int_\Omega \mathbf{N}^{eT}\,\mathrm{d}\mathbf{b}^e\,\mathrm{d}\Omega + \int_{\Gamma_\mathrm{t}} \mathbf{N}^{eT}\,\mathrm{d}\bar{\mathbf{t}}^e\,\mathrm{d}\Gamma, \tag{52}$$

$$\mathrm{d}\mathbf{f}^{e}_{w,\mathrm{ext}} = \mathbf{0}, \tag{53}$$

where the incremental forces $\mathrm{d}\mathbf{f}^{e}_{w,\mathrm{ext}}$, introduced at the discontinuity, are assumed to be zero. From Eqs. (45)–(50), it is clear that a symmetric formulation is obtained, as long as matrices $\mathbf{D}^{e}$ and $\mathbf{T}^{e}$ are symmetric.

At this stage, two different approaches can be adopted:

(i) either the additional nodes are considered as internal nodes in the element, or
(ii) the new nodes are global.

In the former approach, which can be considered a natural extension of the usual embedded discontinuity formulation, condensation of the corresponding additional degrees of freedom can be performed at element level and the bandwidth of the global stiffness matrix is kept fixed during the calculations. In fact, from the second equation of (45):

$$\mathrm{d}\mathbf{w}^{e} = \left[\mathbf{K}^{e}_{ww} + \mathbf{K}^{e}_{\mathrm{d}}\right]^{-1}\left[\mathbf{K}^{e}_{wa}\,\mathrm{d}\mathbf{a}^{e}\right], \tag{54}$$

and substituting $d\mathbf{w}^{e}$ into the first equation of (45) we obtain

$$\left[\mathbf{K}^{e}_{aa} - \mathbf{K}^{e}_{aw}(\mathbf{K}^{e}_{ww} + \mathbf{K}^{e}_{\mathrm{d}})^{-1}\mathbf{K}^{e}_{wa}\right]\mathrm{d}\mathbf{a}^{e} = \mathrm{d}\mathbf{f}^{e}_{\mathrm{ext}}, \tag{55}$$

which allows the definition of the condensed incremental stiffness matrix, given by

$$\mathbf{K}^{e}_{\mathrm{con}} = \left[\mathbf{K}^{e}_{aa} - \mathbf{K}^{e}_{aw}(\mathbf{K}^{e}_{ww} + \mathbf{K}^{e}_{\mathrm{d}})^{-1}\mathbf{K}^{e}_{wa}\right]. \tag{56}$$

Note that no continuity of the jumps across the element boundaries is achieved in this case. However, similar to the works presented in Alfaiate et al. (1992, 1997), Alfaiate and Pires (1998, 1999, 2001), where interface elements were used, the following approximation can be considered: at each element boundary where two internal nodes coincide, the mean values of the corresponding jump components are adopted as the *true* jump components and used in the traction-jump law (see Fig. 3).

In approach (ii), which is adopted here, the additional nodes are global and therefore the bandwidth of the global stiffness matrix increases during the calculations. Nevertheless, for $n_w \geqslant 2$ continuity of the jumps at the discontinuities is automatically enforced across the element boundaries. Moreover, since the jump is continuously distributed over the entire element Ω^{e}, the elements remain conform.

As previously stated in de Borst et al. (2001), this formulation is kinematically similar to a smeared approach. Nevertheless, it should be stressed that the constitutive relation adopted for the continuum is not

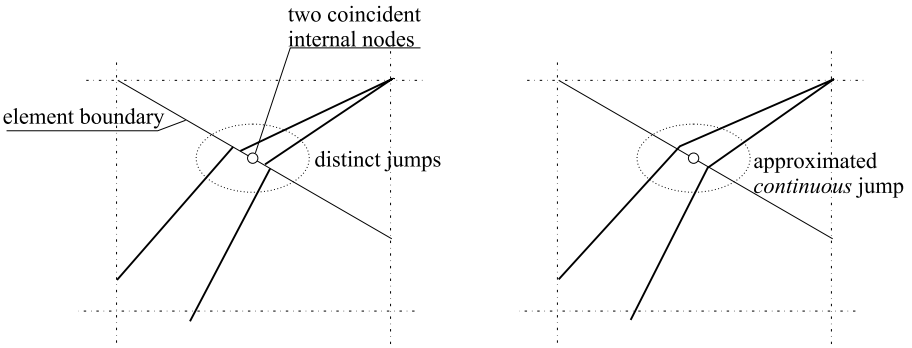

Fig. 3. Approximated *continuous* jump across an element boundary.

modified; instead, a discrete relation is enforced separately at Γ_d (44), whose location and corresponding displacement jumps are known (see also Alfaiate and Sluys, 2002).

5. Material and numerical models

In this section, the material and numerical models are described. A linear elastic bulk behaviour is adopted whereas a localized damage model is used for the traction-jump law. An isotropic law is adopted:

$$\mathbf{t} = (1-d)\mathbf{T}_{el}\mathbf{w}, \tag{57}$$

where $0 \leqslant d \leqslant 1$ is a scalar damage variable and $\mathbf{T}_{el}$ is the *elastic* constitutive tensor in which non-diagonal terms are zero and diagonal terms are penalty functions used to prevent overlapping of crack faces under crack closure. The evolution of damage is given by:

$$d = d(\kappa) = 1 - \exp\left(-\frac{f_t}{G_F}\kappa\right), \tag{58}$$

where k is a scalar variable taken equal to the maximum positive normal jump component:

$$k = \max\langle w_n \rangle^+, \quad \kappa \geqslant 0, \quad \dot{\kappa} \geqslant 0, \tag{59}$$

f_t is the tensile strength and G_F is the fracture energy. A loading function is defined as

$$f = w_n - \kappa. \tag{60}$$

Only mode I opening is considered, i.e. discontinuities open perpendicularly to the direction of the maximum principal stress σ_I whenever

$$\sigma_I = f_t. \tag{61}$$

No shear tractions are allowed at the discontinuities during crack evolution.

5.1. Embedded discontinuity technique

Within the scope of the numerical implementation, it is useful to distinguish between: (i) crack propagation and (ii) crack opening:

(i) a new embedded discontinuity always crosses the entire parent element. Only straight discontinuities are allowed and the corresponding directions are defined perpendicular to the directions of σ_I which is obtained at the central integration point of the parent element.
(ii) The opening criterion (61) should be verified at the crack tip. The crack tip usually lies within the parent element and the corresponding jump, as well as the jump ahead of the crack tip (within the same element), are enforced to be practically zero through the use of the penalty functions in $\mathbf{T}$.

Once a discontinuity is embedded in the parent element, one can rely on the tractions measured at the interface. For instance, for a linear interface (two nodes), the jumps are linear so that the crack tip, which is defined at a location where the opening criterion is verified (where the normal traction component equals f_t in the case of mode I fracture), is usually located inside the parent element since the discontinuity already opened at the node behind the tip and the other node, ahead, is still enforced to be *closed* by using penalty functions in $\mathbf{T}$. If more nodes are adopted for the interface, the tip will also be usually located between two adjacent nodes, thus, inside the element. A new discontinuity is introduced in a next element only when the crack tip approaches the element boundary. At this point, where a node is defined, a correct account of the

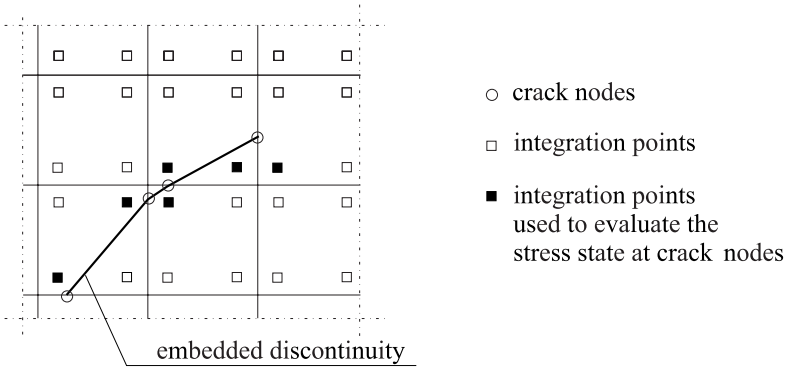

Fig. 4. The stress components at each crack node are taken as the average stress components obtained at the two nearest integration points.

stress state must be obtained, in order to properly fulfill the opening criterion (61). Only one embedded discontinuity is allowed in each element and crack path continuity is achieved according to an algorithm similar to the one presented in Alfaiate et al. (2001a).

Different criteria have been proposed in literature for obtaining the stresses at the crack tip, which give rise to a more or less localized crack evolution criterion, depending on the degree of mesh refinement and on the order of the parent elements. In particular, the following examples are mentioned:

(1) the accurate definition of the stresses near the crack tip is approximated by using special functions taken from linear elastic fracture mechanics (Ingraffea, 1989; Carpinteri et al., 1989; Möes et al., 1999),
(2) the mean values of the stress components obtained at the nearest integration points of the crack tip define the stress state adopted for crack evolution (Alfaiate et al., 1997; Alfaiate and Pires, 1999), or
(3) a *non-local* stress state is adopted near the crack tip,in which case the averaging support is extended beyond the element size (de Borst et al., 2001; Wells, 2001).

Here, similar to the work presented in Alfaiate et al. (1997) and Alfaiate and Pires (1999), the stress components at each crack node are taken as the average stress components obtained at the two nearest integration points, located at each side of the common element boundary (see Fig. 4).

6. Numerical examples

The numerical examples presented are: simple one element examples, a three point bending beam and a single edge notched beam.

6.1. One element examples

The first example is a constant strain triangle, submitted to tension. Due to the asymmetry, the horizontal discontinuity, introduced at the centroid, opens at one of the edges only, as depicted in Fig. 5 where the deformed meshes obtained from both the embedded discontinuity example and a discrete-interface test are presented. In Fig. 6, a perfect match between the load–displacement curves obtained with the two approaches is presented. Note that a homogeneous jump field across the element would be obtained with the non-symmetric formulation used in Armero and Garikipati (1996), Oliver (1996a,b), Wells and Sluys (2000, 2001b), Alfaiate et al. (2001a), yielding more dissipation of energy.

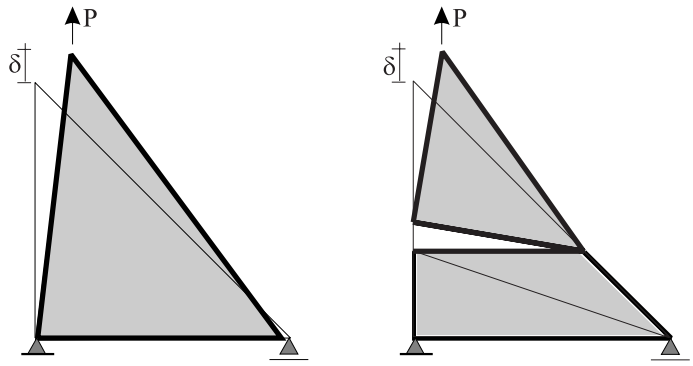

Fig. 5. Asymmetric triangle submitted to tension.

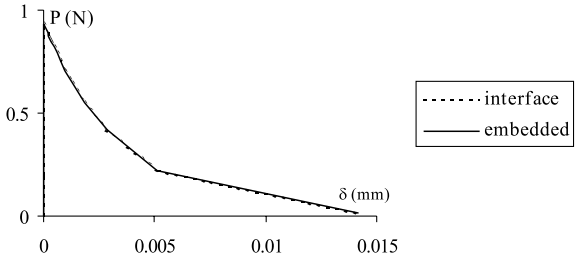

Fig. 6. Load–displacement curves corresponding to Fig. 5.

Next, a symmetric triangle is submitted to tension. Depending on the position of the prescribed discontinuity, different maximum loads are obtained, exactly in the same way as in a discrete-interface approach. In Fig. 7, the load–displacement curves obtained with the embedded model and with the interface approach are presented, which show almost complete similarity. Note that, if the non-symmetric formu-

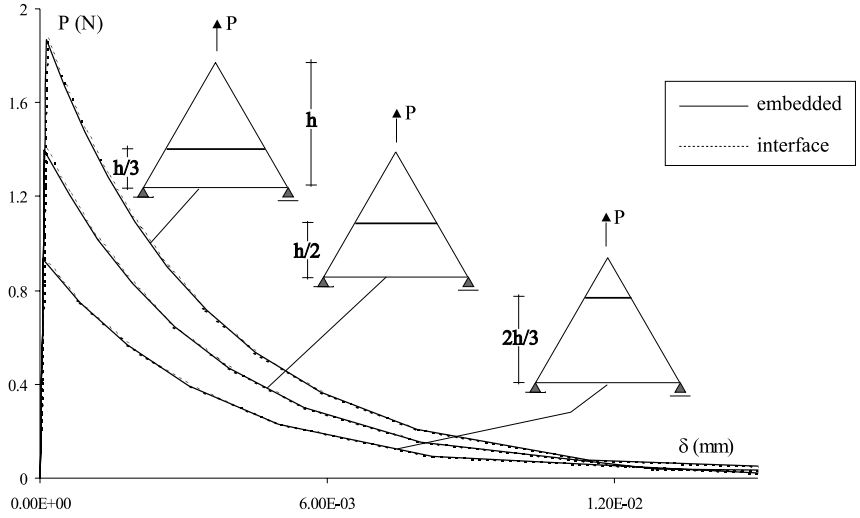

Fig. 7. Symmetric triangle submitted to tension.

lation were adopted (Oliver, 1996b), since it does not depend on the crack length, the same peak load (as well as load–displacement curve) would be obtained in the three examples.

6.2. Three point bending beam

The three point bending beam test is another example in which the discrete-interface and the embedded approach were compared. The beam dimensions are: length = 2 m, thickness = 0.05 m and depth = 0.2 m, with a 0.1 m notch depth. The adopted material parameters are: $f_t = 3.33$ MPa, Young modulus $E = 30$ GPa and fracture energy $G_F = 115$ N/m. In Fig. 8, the deformed meshes obtained with both approaches are presented. In Fig. 9, the load–displacement curves numerically obtained are presented and compared to the experimental result reported in Petersson (1981). First, a prescribed vertical crack path is introduced in both the embedded and the discrete-interface numerical examples. In this case, the location and orientation

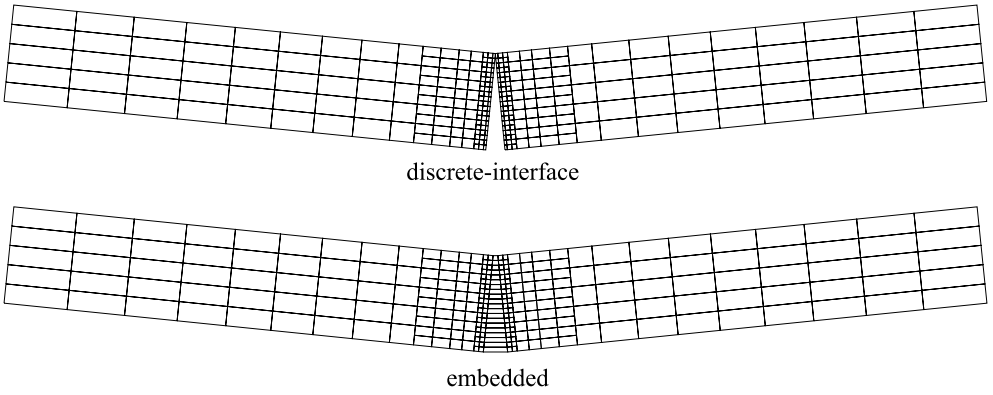

Fig. 8. Three point bending beam: deformed meshes.

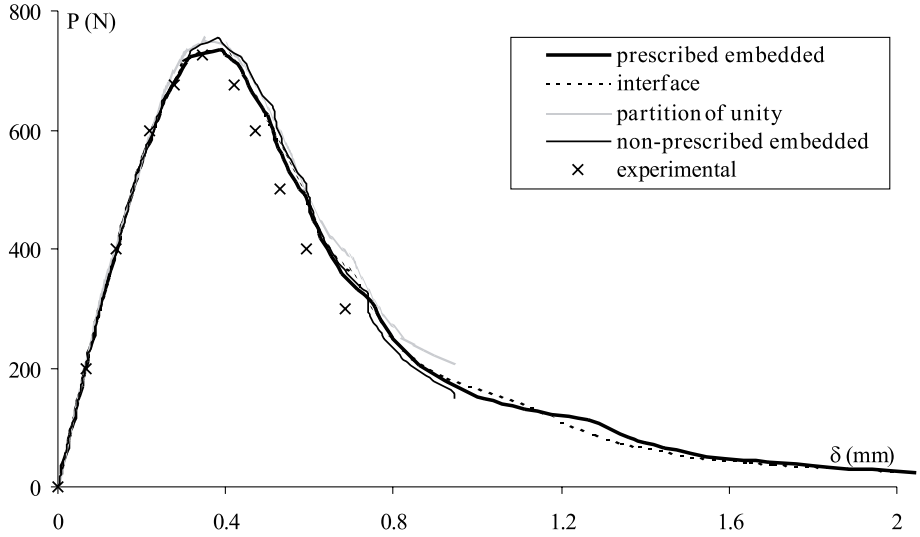

Fig. 9. Three point bending beam: load–displacement curves.

of the discontinuities are given a priori, such that the crack path in enforced along the midspan, both in the embedded and in the interface analyses. Then, a solution with non-prescribed embedded discontinuities is also obtained. In the latter example, as a first attempt of a simplified opening criterion, the stress state at the crack tip is obtained at the centre of the element ahead of the crack tip. As a result, compared to the prescribed solutions, the crack tip always opens later and a higher peak load than the experimental one is obtained. The result obtained with the the partition of unity method is also shown, where the same opening criterion is adopted, thus leading to a solution with delayed crack propagation similar to the non-prescribed one.

6.3. Single edge notched beam

The last test presented is the single edge notched beam. The beam dimensions and boundary conditions are shown in Fig. 11. The adopted material parameters are: $f_t = 2.8$ MPa, Young modulus $E = 35$ GPa and fracture energy $G_F = 100$ N/m. In Schlangen (1993), Schlangen and van Mier (1993) experimental results were obtained with this beam, in which the load is controlled such that a monotonic increasing of the sliding of the notch (crack mouth sliding displacement, CMSD) is enforced. In the numerical analyzes, load control is performed using an arc length method where only the relative sliding displacement of the notch (CMSD) is taken into account in the constraint equation.

Four different numerical solutions are presented: in the first three analyses a structured mesh with four node isoparametric elements is used, whereas in the fourth analysis an unstructured mesh is adopted with constant strain triangles. In all cases, continuity of the crack path is enforced.

6.3.1. Structured mesh

In Fig. 10 the load–CMSD curves obtained with a structured mesh with quadrilateral elements are compared to the experimental load–CMSD curve. In test number one (curve 1), a non-prescribed numerical solution was obtained adopting the simplified opening criterion mentioned for the three-point bending

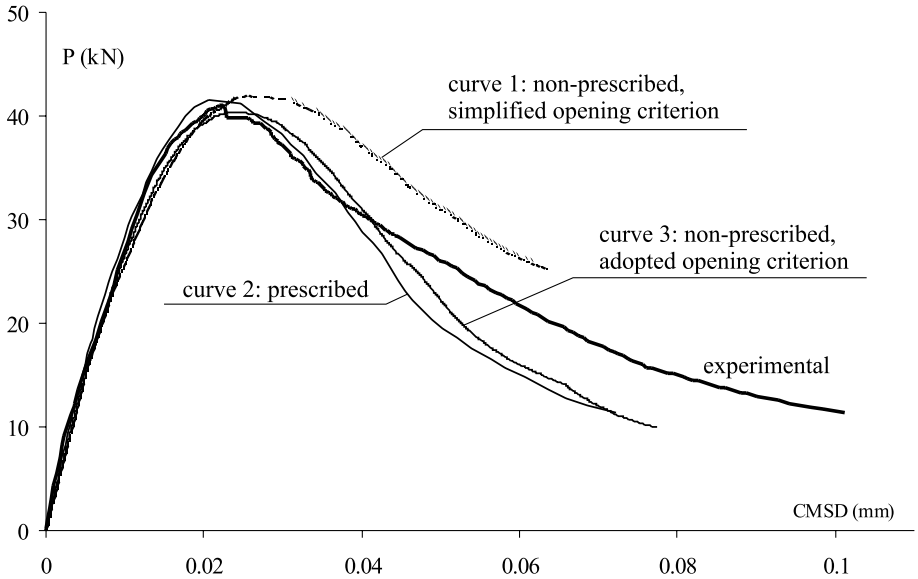

Fig. 10. Structured mesh: load–CMSD curves.

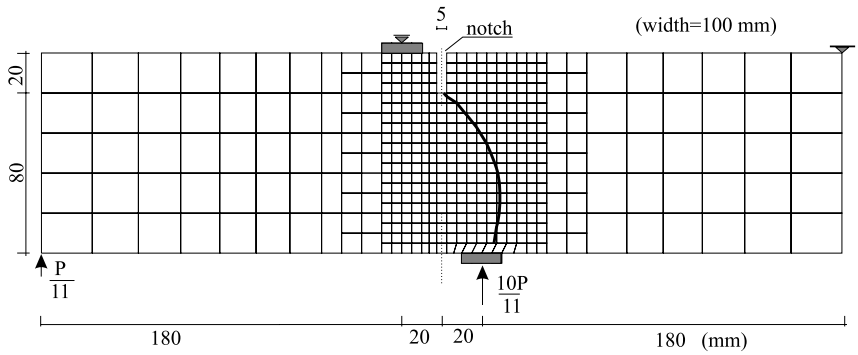

Fig. 11. Single end notched beam: crack path with structured mesh from test number three.

beam. It is clear that the solution obtained with this criterion deviates from the experimental result. In test number two the crack path was prescribed (curve 2). In this case, the information relative to the location and orientation of the cracks, which had to be known a priori, was taken from the first test. In test number three (curve 3), a better account of the stresses at the crack tip was adopted by means of the opening criterion defined in Section 5.1. It is obvious that this criterion gives rise to a load–CMSD curve similar to the curve obtained with the prescribed crack and that both curves agree well with the experimental one. In Fig. 11 the crack path obtained from test number three is shown. In Fig. 12(a) the corresponding deformed mesh is presented; in Fig. 12(b) the same deformed mesh is shown where the elements crossed by the

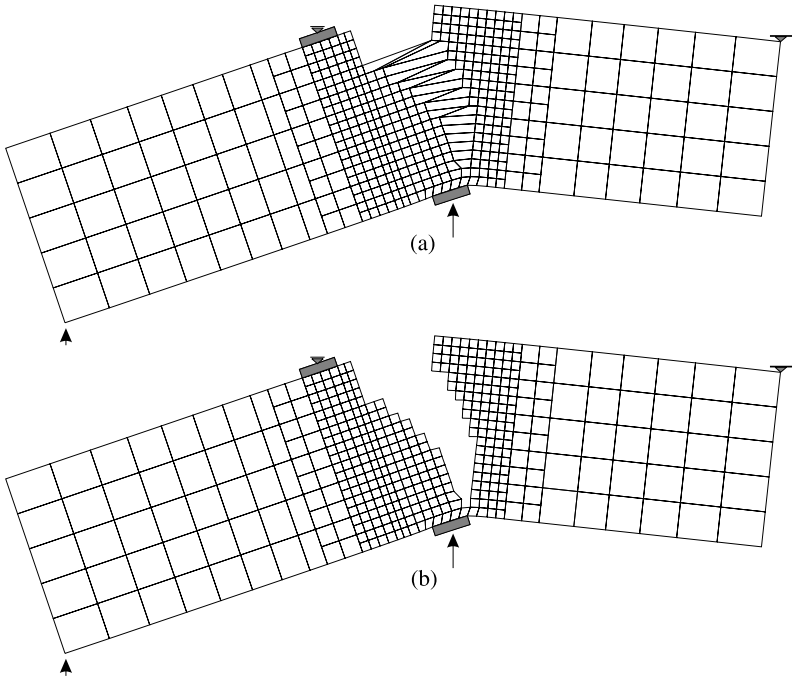

Fig. 12. Single edge notched beam: deformed mesh obtained from test number three; in (b) the elements crossed by the discontinuity were artificially removed.

discontinuity were artificially removed. Both the crack path and the deformed mesh agree well with the experimental observation reported in Schlangen and van Mier (1993), Schlangen (1993), in spite of the fact that the adopted mesh is relatively coarse (about 350 elements).

6.3.2. Unstructured mesh

In Fig. 13, the load–CMSD curve obtained with the unstructured mesh (curve 4) is compared to the experimental curve. In this figure, the result taken from Alfaiate et al. (2001a) is also presented (curve 5). This result was obtained with the non-symmetric formulation (Armero and Garikipati, 1996; Oliver, 1996a,b; Wells and Sluys, 2000, 2001b) with the enforcement of crack path continuity. It is interesting to see that the ascending branch is better approximated with the new formulation (curve 4) than with the non-symmetric approach (curve 5), although the peak load is still larger than the experimentally observed peak load. However, it should be mentioned that CST elements can not provide a correct definition of the stresses at crack nodes, unless a much refined mesh is used, which is not the case here. In Fig. 14, the crack path obtained from test number four is shown.

Finally, it is interesting to note that curves 2–5 in Figs. 10 and 13 show a more brittle softening branch than the experimental curve. This is due to the fact that mixed mode fracture was neglected, i.e., no shear tractions were allowed at the discontinuities during crack evolution. In fact, in Alfaiate et al. (2001a,b) it was shown the response becomes more ductile if more shear tractions are allowed in the discontinuities during crack opening.

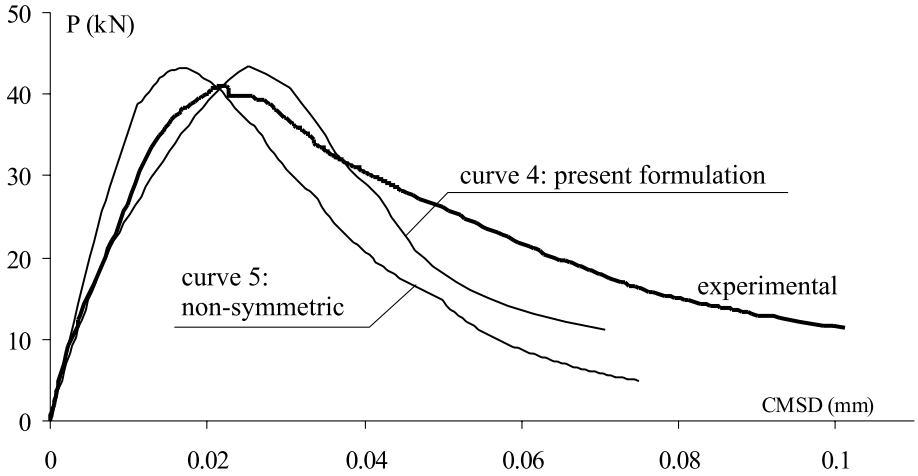

Fig. 13. Unstructured mesh: load–CMSD curves.

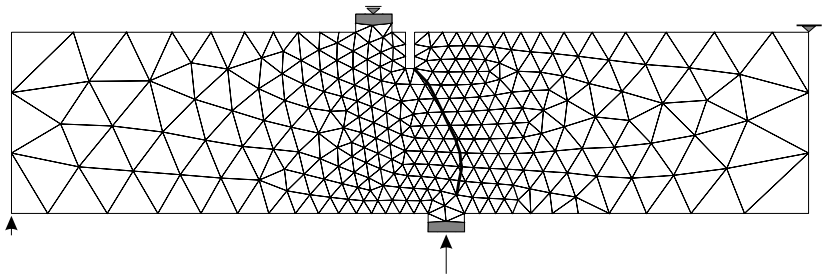

Fig. 14. Single edge notched beam: crack path obtained with unstructured mesh.

7. Conclusions and discussion

In this paper, a new numerical implementation of embedded discontinuities with non-homogeneous jumps across the elements was introduced. The comparison with other embedded and partition-of-unity approaches was carried out. The important conclusions of this study are:

(1) in the adopted formulation, the jumps are approximated by additional degrees of freedom obtained at additional nodes;
(2) these degrees of freedom can be considered either as global or local:
   (a) in the former case, which is adopted in the paper, new global degrees of freedom are introduced as the crack propagates, allowing for continuous jumps across element boundaries, at the cost of an increasing bandwidth of the stiffness matrix;
   (b) in the latter case, which can be considered an extension of previous embedded discontinuity approaches, the jumps are considered as internal degrees of freedom, which can be condensed out at element level, thus keeping the stiffness bandwidth constant. However, in this case, continuity of the displacement jumps across element boundaries can not be enforced;
(3) the variational formulation adopted consists of the principle of virtual work applied to a body crossed by a discontinuity, as previously presented in Malvern (1969);
(4) it is shown that, essentially, the same variational formulation is adopted in other approaches, such as the partition of unity method or extended finite elements, and the embedded formulation introduced by Lotfi and Shing (1995);
(5) it is also shown that, similar to the work of Simo et al. (1993), in which a non-symmetric formulation is introduced, the traction continuity condition is also imposed in a weak form, which yields, although in a different way, a symmetric formulation;
(6) the adopted formulation is found similar to a formulation with interface elements, although the jumps are projected (*smeared*) to the element nodes using the regular shape functions, as done in other embedded approaches and in the partition of unity and XFEMs;
(7) in the partition of unity and XFEMs, the approximation of the enhanced displacement field is introduced directly at the existing element nodes; in the present approach, the enhanced degrees of freedom at the nodes are derived from the jumps measured at the discontinuity surface Γ_d, which is *embedded* in the parent element;
(8) the formulation adopted depends not only on the derivatives of the enhanced degrees of freedom (symmetric and non-symmetric formulations with constant jumps), but also on the relative displacements, comparable to the partition of unity method;
(9) promising results were obtained with relatively coarse structured and non-structured meshes which compare well with experimental results and with the results obtained from analyses with interface elements.

References

Alfaiate, J., Pires, E.B., 1998. Mode I and mixed mode non-prescribed discrete crack propagation in concrete. In: Mihashi, H., Rokugo, K. (Eds.), Fracture Mechanics of Concrete Structures—FRAMCOS3, vol. 2, AEDIFICATIO, Gifu, Japan, pp. 739–748.

Alfaiate, J., Pires, E.B., 1999. A discrete crack numerical model. In: Carpinteri, A., Aliabadi, M. (Eds.), Computational Fracture Mechanics in Concrete Techonology. WIT Press/Computational Mechanics Publications, Southampton, UK, pp. 133–162.

Alfaiate, J., Pires, E.B., 2001. Evolução da fissuração num túnel de betão. Revista Internacional de Métodos Numéricos para Cálculo y Diseño en Ingeniería 17, 185–197.

Alfaiate, J., Pires, E.B., Martins, J.A.C., 1992. A finite element model for the study of crack propagation. In: Aliabadi, M.H., Cartwright, D.J., Nisitani, H. (Eds.), 2nd International Conference on Localised Damage. Computational Mechanics Publications and Elsevier Applied Science, Southampton, UK, pp. 261–282.

Alfaiate, J., Pires, E.B., Martins, J.A.C., 1997. A finite element analysis of non-prescribed crack propagation in concrete. Computers and Structures 63 (1), 17–26.

Alfaiate, J., Sluys, L.J., 2002. Analysis of a compression test on concrete using strong embedded discontinuities. In: Mang, H., Rammerstorfer, F., Eberhardsteiner, J. (Eds.), WCCM V, Fifth World Congress on Computational Mechanics, Vienna, Austria. Available from <http://wccm.tuwien.ac.at>.

Alfaiate, J., Wells, G.N., Sluys, L.J., 2001a. On the use of embedded discontinuity elements with crack path continuity for mode I and mixed mode fracture. Engineering Fracture Mechanics 69 (6), 661–686.

Alfaiate, J., Wells, G.N., Sluys, L.J., 2001b. Strong embedded discontinuities for simulating fracture in quasi-brittle materials. In: de Borst, R., Mazars, J., Pijaudier-Cabot, G., van Mier, J.G.M. (Eds.), Fracture Mechanics of Concrete Structures—FRAMCOS4, Paris, France, pp. 749–756.

Armero, F., Garikipati, K., 1996. An analysis of strong discontinuities in multiplicative finite strain plasticity and their relation with the numerical simulation of strain localization. International Journal of Solids and Structures 33 (20–22), 2863–2885.

Babuška, I., Melenk, J.M., 1997. The partition of unity method. International Journal for Numerical Methods in Engineering 40 (4), 727–758.

Borja, R.I., 2000. A finite element model for strain localization analysis of strongly discontinuous fields based on standard galerkin approximation. Computer Methods in Applied Mechanics and Engineering 190, 1529–1549.

Carpinteri, A., Valente, S., Bocca, P., 1989. Mixed mode choesive crack propagation. In: Salama, K., Ravi-Chandar, K., Taplin, D., Rao, P.R. (Eds.), 7th Int. Conf. on Fracture (ICF-7). Pergamon Press, New York, USA, pp. 2243–2257.

de Borst, R., Wells, G.N., Sluys, L.J., 2001. Some observations on embedded discontinuity models. Engineering Computations 18 (1–2), 241–254.

Duarte, C.A., Oden, J.T., 1996. H-p clouds—an h-p meshless method. Numerical Methods for Partial Differential Equations 12 (6), 673–705.

Dvorkin, E.N., Cuitino, A.M., Goia, G., 1990. Finite elements with displacement interpolated embedded localization lines insensitive to mesh size and distortions. International Journal for Numerical Methods in Engineering 30, 541–564.

Ingraffea, A., 1989. Shear cracks. In: Elfgren, L. (Ed.), Fracture Mechanics of Concrete Structures—From Theory to Applications, report of the Technical Committee 90-FMA Fracture Mechanics of Concrete-Applications. Chapman and Hall, London, UK, pp. 231–233.

Jirásek, M., 2000. Comparative study on finite elements with embedded discontinuities. Computer Methods in Applied Mechanics and Engineering 188, 307–330.

Jirásek, M., Zimmermann, T., 2001a. Embedded crack model: I. Basic formulation. International Journal for Numerical Methods in Engineering 50, 1269–1290.

Jirásek, M., Zimmermann, T., 2001b. Embedded crack model. Part II: Combination with smeared cracks. International Journal for Numerical Methods in Engineering 50, 1291–1305.

Klisinski, M., Runesson, K., Sture, S., 1991. Finite element with inner softening band. ASCE Journal of Engineering Mechanics 117 (3), 575–587.

Larsson, R., Runesson, K., 1996. Element-embedded localization band based on regularized displacement discontinuity. ASCE Journal of Engineering Mechanics 122 (5), 402–411.

Lotfi, H.R., Shing, P.B., 1995. Embedded representation of fracture in concrete with mixed finite elements. International Journal for Numerical Methods in Engineering 38 (8), 1307–1325.

Malvern, L.E., 1969. Introduction to the Mechanics of a Continuous Medium. Prentice-Hall International, New Jersey.

Melenk, J.M., Babuška, I., 1996. The partition of unity finite element method: basic theory and applications. Computer Methods in Applied Mechanics and Engineering 139 (1–4), 289–314.

Möes, N., Dolbow, J., Belytschko, T., 1999. A finite element method for crack growth without remeshing. International Journal for Numerical Methods in Engineering 46 (1), 131–150.

Ohlsson, U., Olofsson, T., 1997. Mixed-mode fracture and anchor bolts in concrete analysis with inner softening bands. ASCE Journal of Engineering Mechanics 123, 1027–1033.

Oliver, J., 1996a. Modelling strong discontinuities in solid mechanics via strain softening constitutive equations. Part 1: Fundamentals. International Journal for Numerical Methods in Engineering 39 (21), 3575–3600.

Oliver, J., 1996b. Modelling strong discontinuities in solid mechanics via strain softening constitutive equations. Part 2: Numerical simulation. International Journal for Numerical Methods in Engineering 39 (21), 3601–3623.

Petersson, P.E., 1981. Crack growth and development of fracture zones in plain concrete and similar materials. Ph.D. thesis, Lund Institute of Technology, Sweden.

Schlangen, E., 1993. Experimental and numerical analysis of fracture processes in concrete. Ph.D. thesis, Delft University of Technology.

Schlangen, E., van Mier, J.G., 1993. Mixed-mode fracture propagation: a combined numerical and experimental study. Fracture and Damage of Concrete and Rock, 166–175.

Simo, J.C., Oliver, J., Armero, F., 1993. An analysis of strong discontinuities induced by strain-softening in rate-independent inelastic solids. Computational Mechanics 12, 277–296.

Simone, A., Remmers, J.J.C., Wells, G.N., 2000. An interface element based on the partition of unity. Tech. Rep. CM2001.007, Technical University of Delft, Delft, The Netherlands.

Washizu, K., 1982. Variational Methods in Elasticity and Plasticity, third ed. Pergamon Press Ltd, Oxford.

Wells, G., 2001. Discontinuous modelling of strain localisation and failure. Ph.D. thesis, Delft University of Technology.

Wells, G.N., Sluys, L.J., 2000. Analysis of slip planes in three-dimensional solids. Computer Methods in Applied Mechanics and Engineering 190 (28), 3591–3606.

Wells, G.N., Sluys, L.J., 2001a. A new method for modelling cohesive cracks using finite elements. International Journal for Numerical Methods in Engineering 50 (2), 2667–2682.

Wells, G.N., Sluys, L.J., 2001b. Three-dimensional embedded discontinuity model for brittle fracture. International Journal of Solids and Structures 38 (5), 897–913.